

DM3D: Deformable Mamba via Offset-Guided Gaussian Sequencing for Point Cloud Understanding

Bin Liu, Chunyang Wang*, Xuelian Liu
Xi'an Technological University

liubin@st.xatu.edu.cn, {Wangchunyang, Liuxuelian}@xatu.edu.cn

Abstract

State Space Models (SSMs) demonstrate significant potential for long-sequence modeling, but their reliance on input order conflicts with the irregular nature of point clouds. Existing approaches often rely on predefined serialization strategies, which cannot adjust based on diverse geometric structures. To overcome this limitation, we propose **DM3D**, a deformable Mamba architecture for point cloud understanding. Specifically, DM3D introduces an offset-guided Gaussian sequencing mechanism that unifies local resampling and global reordering within a deformable scan. The Gaussian-based KNN Resampling (GKR) enhances structural awareness by adaptively reorganizing neighboring points, while the Gaussian-based Differentiable Reordering (GDR) enables end-to-end optimization of serialization order. Furthermore, a Tri-Path Frequency Fusion module enhances feature complementarity and reduces aliasing. Together, these components enable structure-adaptive serialization of point clouds. Extensive experiments on benchmark datasets show that DM3D achieves state-of-the-art performance in classification, few-shot learning, and part segmentation, demonstrating that adaptive serialization effectively unlocks the potential of SSMs for point cloud understanding.

1. Introduction

3D point clouds serve as a sparse yet efficient representation of real-world geometry and are widely used in numerous vision applications, such as autonomous driving [35, 46, 48], robotics [5], and AR [18]. Unlike structured 2D images, point clouds lack a regular grid structure, meaning there is no inherent spatial adjacency between points, which poses fundamental challenges to effective representation and semantic understanding [3, 17, 36, 49, 51]. Recently, Mamba enhanced State Space Models (SSMs) [11] with a selective mechanism, achieving remarkable computational efficiency and strong long-sequence modeling capability. However,

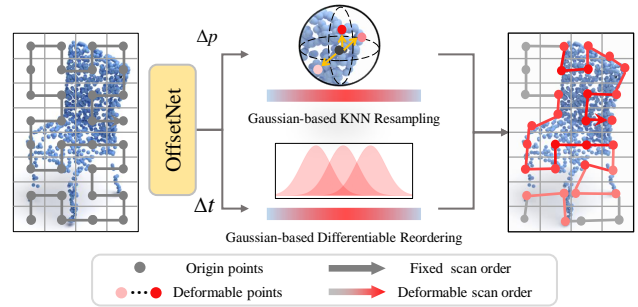


Figure 1. **Illustration of our deformable scanning.** The offset network predicts spatial offsets Δp and sequential offsets Δt . Guided by the predicted offsets, a Gaussian kernel performs consistent local resampling and global reordering, yielding structure-aware sequences that capture fine-grained geometric details.

applying Mamba [10] to point clouds requires a crucial step—serialization—which plays a key role in enabling the model to capture the underlying spatial structure.

A variety of strategies have been explored to serialize point clouds for sequential modeling, including space-filling curves (SFCs) [17, 43, 49], MLP-based projections [13, 20], and voxel- or graph-based unfoldings [6, 34]. Despite their differences, these approaches share a common limitation: once serialization is completed, the token order becomes static and remains agnostic to both the input geometry and the downstream task. Such rigidity simplifies token feeding into SSMs but fundamentally contradicts the irregular and permutation-invariant nature of point clouds. Consequently, spatially adjacent points may be scattered throughout the sequence, disrupting local continuity and hindering the capture of meaningful structural details, especially in sparse or complex regions.

In contrast, human vision adaptively attends to geometric edges, local details, and structural cues, extracting the most informative patterns under limited attention. This content-aware perception efficiently forms discriminative and relational representations. Inspired by this mechanism, we inquire: can a model dynamically adjust its scanning path to

the geometric structure of a point cloud, thereby endowing SSMs with genuine structural awareness? A recent effort, DefMamba [22], takes a initial step in this direction by incorporating deformable mechanisms into SSMs, where spatial and sequential offsets are learned to adjust scanning paths. However, its design is confined to 2D regular grids, where scanning corresponds merely to reordering predefined token indices [14, 24, 42, 54]. Point clouds, in contrast, lack an inherent order. Thus, deformable scanning is not merely a simple reordering of tokens, but a structure-aware sequence construction that demands joint spatial adaptivity and dynamic serialization.

To this end, **we propose DM3D (Deformable Mamba for 3D point clouds)**, which, to our knowledge, is the first work to integrate a deformable mechanism tailored for point cloud understanding into Mamba. The core idea is to employ learnable spatial and sequential offsets to guide the Gaussian weighting, thereby achieving dual-domain deformation that unifies spatial and sequential adaptivity (see Fig. 1). Our key contributions are:

- We introduce a deformable mechanism that dynamically adapts scanning paths based on input geometry, enhancing the capture of fine-grained geometric details.
- We propose an offset-guided Gaussian sequencing mechanism that unifies local resampling and global reordering within the deformable scan. Its Gaussian-based KNN Resampling (GKR) enhances local structural awareness through adaptive neighbor aggregation, while the Gaussian-based Differentiable Reordering (GDR) enables end-to-end optimization of token sorting.
- We propose a Tri-Path Frequency Fusion (TPFF) module that adaptively exchanges information across paths and suppresses information redundancy.

2. Related Work

Serialization and Mamba for Point Cloud. Point cloud serialization aims to convert unordered point sets into structured sequences compatible with sequence models. Previous methods generate sequences based on predefined traversal rules and process them with Transformer-based architectures [6, 25, 39]. As point cloud sequences become longer, Transformers [32] encounter significant computational bottlenecks. In contrast, Mamba, with its linear complexity, can handle such sequences efficiently [13, 27, 43, 44]. However, its effectiveness depends on maintaining the adjacency of semantically or spatially related points in the sequence [16, 26, 43, 47]. Thus, serialization serves as a crucial bridge between point clouds and Mamba, and different serialization schemes may be better suited to different tasks.

PointMamba [17] employs Hilbert and transposed Hilbert curves for efficient sequence generation, preserving spatial locality and providing a simple yet effective baseline. PCM [49] introduces a consistent traversal strat-

egy, generating multiple sequence variants along coordinate axes and optimizing local continuity using order prompts. VoxelMamba [47] serializes voxelized scenes using Hilbert curves to maintain neighborhood consistency, while GridMamba [43] fuses multiple SFCs and randomly alternates them across layers to alleviate locality loss.

Despite their flexibility, these approaches rely on static, predefined mapping rules. In contrast, our DM3D treats serialization as a learnable module that allows the model to dynamically optimize point sorting during training, effectively reformulating serialization as a deformable process.

Deformable Mechanisms in Visual Tasks. Deformable mechanisms enable models to dynamically adjust their receptive fields according to input content. The concept originated from DCN [7], which introduced learnable offsets to adapt convolutional sampling locations. DAT [41] later extended this idea into the attention mechanism. In point cloud understanding, PointConv [37] incorporated deformable continuous convolution to handle non-uniform point distributions, while KPConv [30] further learned kernel displacements to better adapt to diverse local geometries. 3D-GCN [19] combined deformable kernels with graph convolution to achieve translation and scale invariance. CenterFormer [53] and PTV2 [38] respectively leveraged deformable attention for efficient multi-scale feature aggregation and spatial alignment in detection and segmentation tasks, achieving notable performance gains. Previous deformable designs have enabled CNNs and Transformers to adapt sampling positions in the spatial domain. In contrast, DM3D extends deformability to the sequence domain, enabling SSMs to adapt the serialization order based on point cloud geometry.

3. Method

3.1. Preliminary

State Space Models (SSMs) are sequence modeling frameworks derived from linear time-invariant systems in control theory, capturing dependencies through latent state transitions. To adapt SSMs for discrete sequence modeling, Structured SSMs [12] (S4) employ the Zero-Order Hold (ZOH) method for discretization, introducing a timescale parameter Δ . The discretized equations are:

$$\bar{A} = \exp(\Delta A), \bar{B} = \Delta A^{-1}(\exp(\Delta A) - I)\Delta B \quad (1)$$

$$h_t = \bar{A}h_{t-1} + \bar{B}u_t, y_t = Ch_t \quad (2)$$

where $\bar{A} \in \mathbb{R}^{L \times L}$ and $\bar{B} \in \mathbb{R}^{L \times 1}$ are the discretized counterparts of continuous state evolution matrix A and input projection matrices B , respectively. C denotes the output projection matrix, and u_t , h_t , and y_t represent the input, hidden state, and output at time step t .

This discrete formulation enables SSMs to model long sequences with linear complexity. Mamba [10] enhances S4

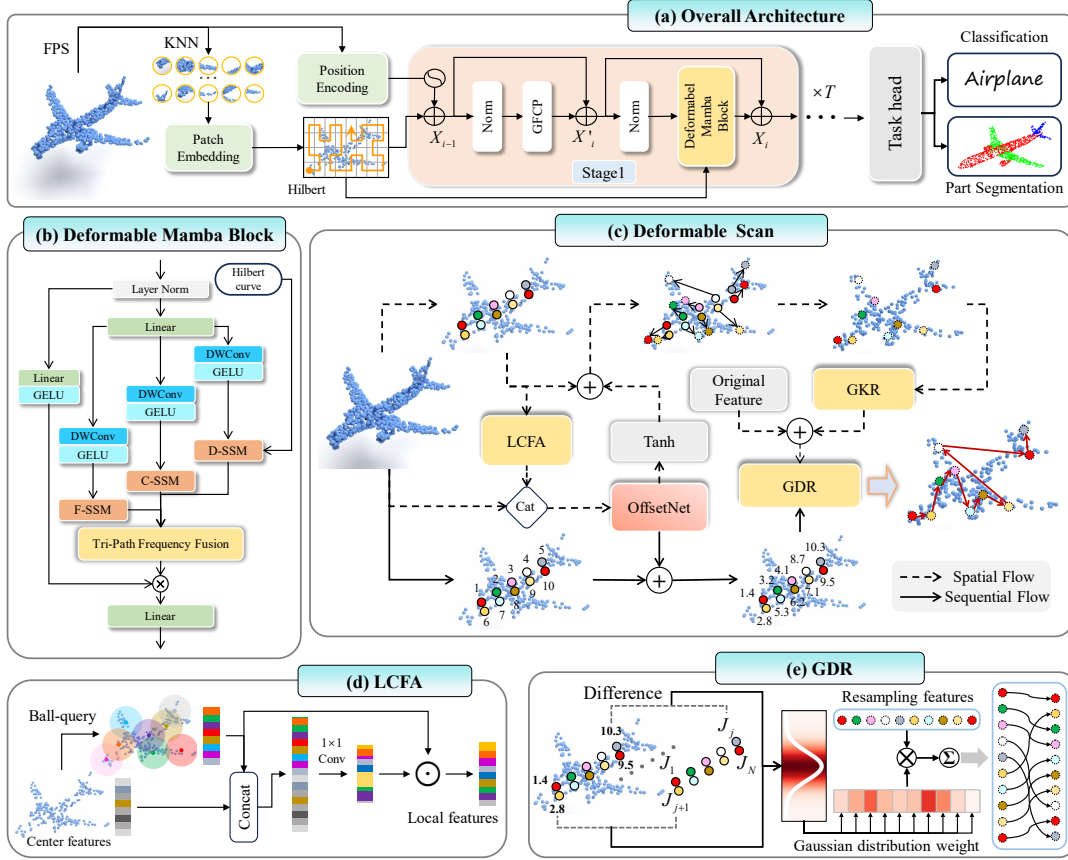


Figure 2. **Overview of DM3D.** (a) **Overall architecture** showing the embedding, encoder, and decoder structures. (b) **The Deformable Mamba Block (DMB)** consists of three SSM branches: the standard forward SSM [42] (F-SSM) branch, the channel-flip backward SSM [13] (C-SSM) branch, and the deformable SSM (D-SSM) branch. (c) **Deformable Scan**, the core of D-SSM, predicts spatial and sequential offsets via OffsetNet, enabling unified Gaussian-based resampling and differentiable reordering. ”Spatial flow” and ”Sequential flow” indicate operations in the spatial and sequence domains, respectively. (d) **LCFA** provides local contextual cues for the offset network. (e) **GDR** performs differentiable token reordering according to learned offsets. **Symbols:** *Cat* and *Concat* denote concatenation along the channel dimension, \odot element-wise multiplication, \oplus residual addition, \otimes matrix multiplication, and \sum summation.

through a Selective Scan (S6) mechanism that renders Δ , B , and C input-dependent, allowing for dynamic adjustment. Coupled with the introduction of a global convolution for efficiency, these improvements establish Mamba as a robust and efficient framework for sequential processing.

3.2. Overview

DM3D adopts a variant of the ViT [15] as its backbone architecture, following the design adopted by baseline networks such as PointBERT [45] and PointMamba [42]. The overall framework is illustrated in Fig. 2(a).

Given an input point cloud, we first apply Farthest Point Sampling (FPS) and K-Nearest Neighbor (KNN) grouping to partition it into N local groups, each containing K points. A lightweight PointNet extracts local features $F \in \mathbb{R}^{N \times D}$, with group centers $P \in \mathbb{R}^{N \times 3}$, where D denotes the embedding dimension. To inject geometric priors, the absolute

coordinates of each center are encoded via an MLP to obtain position embeddings $pos \in \mathbb{R}^{N \times D}$, which are added to the local features. A classification token $F_{cls} \in \mathbb{R}^{1 \times D}$ is prepended, and the resulting embeddings are serialized along a Hilbert curve to form the initial token sequence $X_0 \in \mathbb{R}^{(N+1) \times D}$ for subsequent modeling. Each encoder stage in DM3D follows a Transformer-like architecture consisting of a Geometry-Feature Coupled Pooling (GFPC) module and a Deformable Mamba Block. The GFPC, following HyMamba [20], serves as a local enhancement layer, while the Deformable Mamba Block (DMB) performs deformable state-space modeling. The computation at the i -th stage is formulated as:

$$X_i' = GFPC(LN(X_{i-1})) + X_{i-1}, \quad (3)$$

$$X_i = DMB(LN(X_i')) + X_i' \quad (4)$$

where $X_i \in \mathbb{R}^{(N+1) \times D}$ is the output of the i -th stage and

LN denotes Layer Normalization.

After T encoding stages, the classification token and the average-pooled feature from the final stage are concatenated and fed into a task-specific head.

3.3. Deformable Mamba Block

The Deformable Mamba Block serves as the core of this work, aiming to dynamically adjust the scanning path by reorganizing spatial and sequential structures. As illustrated in Fig. 2(b), following prior works [22, 43, 44], we replace the original 1D causal convolution with depthwise convolution and introduce a D-SSM branch, while retaining the C-SSM branch from Mamba3D [13] and the F-SSM [42] branch to maintain model stability.

Local Context Feature Aggregation (LCFA). The feature representation of a single center point is often insufficient, as geometric relationships in point clouds primarily reside within local neighborhoods. To predict meaningful offsets, it is essential to perceive the surrounding geometric context. As shown in Fig. 2(c), we aggregate features within each neighborhood to capture rich local contextual dependencies.

Specifically, given center points P and their corresponding features F , a ball query with radius r is applied to find neighboring points $\{p_k \mid \|p_k - p_i\| \leq r\}$, forming the neighborhood index set $\mathcal{N}(i)$. The neighborhood coordinates and features are denoted as $p_{\mathcal{N}(i)} \in \mathbb{R}^{N \times K_q \times 3}$ and $F_{\mathcal{N}(i)} \in \mathbb{R}^{N \times K_q \times D}$, where K_q is the number of neighbors.

The center and neighborhood features are concatenated and passed through a 1×1 convolution to produce aggregation weights (see Fig. 2(d)):

$$F_{context} = \sum_{j \in \mathcal{N}(i)} Conv_{1 \times 1}([F_E; F_{\mathcal{N}(i)}]) \cdot F_{\mathcal{N}(i)} \quad (5)$$

where $F_E \in \mathbb{R}^{N \times K_q \times D}$ is the center feature expanded for alignment, and $F_{context}$ denotes the aggregated local contextual representation.

While $F_{context}$ encodes local geometric relationships, it lacks a global understanding of the shape. Relying solely on local features may lead to biased offset predictions. Therefore, we further concatenate it with global features to form the aggregated representation F_{agg} , which serves as the input to the offset network.

Offset-guided Gaussian Weighting. Following the design of DAT [41], we adopt a depthwise separable convolution with a large kernel, followed by ReLU activation and a 1×1 convolution, to predict the initial four-dimensional offsets. A channel attention (CA) module is applied after the convolution to reduce feature redundancy [22]. To prevent excessively large deformations, the offsets are bounded by a hyperbolic tangent function and then decomposed into spa-

tial and sequential components:

$$O_{offset} = Conv_{1 \times 1}(ReLU(CA(DWConv(F_{agg})))) \quad (6)$$

$$O'_{offset} = \tanh(O_{offset}) = [\Delta p; \Delta t] \quad (7)$$

where $\Delta p \in \mathbb{R}^{N \times 3}$ represents spatial offsets for coordinate deformation, and $\Delta t \in \mathbb{R}^{N \times 1}$ denotes sequential offsets for sequence reordering.

The offset operation results in sampled positions that no longer align with the original point set, necessitating both spatial resampling and sequential reordering. We observe that these two operations inherently follow a common principle: points with higher similarity should exert stronger influence during feature aggregation and sequence organization, while the contribution of dissimilar points should gradually decay. Motivated by this, we unify resampling and reordering into a single formulation rather than treating them as independent processes. Specifically, we introduce a mechanism that applies Gaussian kernels of identical form across both spatial and sequential domains, differing only in their operational domains and neighborhood definitions. This unified formulation enables consistent weighting and smoothing for both local resampling and global reordering.

The general Gaussian kernel is defined as:

$$\mathcal{W}(d; \sigma) = \exp\left(-\frac{d^2}{2\sigma^2}\right) \quad (8)$$

where d is the coordinate or index distance, and σ is the corresponding learnable scale for resampling and reordering.

Gaussian-based KNN Resampling (GKR). For resampling, after applying coordinate offsets, each offset point p'_i retrieves its K_r nearest neighbors from the original point set, denoted as the index set $\mathcal{N}_{r(i)} = \{j_1, \dots, j_{K_r}\}$. A batch mask is used to assign infinite distances between points from different batches, ensuring that neighbor search occurs only within the same batch.

For each offset point p'_i , feature interpolation is performed within its KNN neighborhood $\mathcal{N}_{r(i)}$:

$$p'_i = p_i + \Delta p_i \quad (9)$$

$$f'_i{}^{(s)} = \sum_{j \in \mathcal{N}_{r(i)}} \frac{\mathcal{W}(\|p'_i - p_j\|_2; \sigma_s)}{\sum_{l \in \mathcal{N}_{r(i)}} \mathcal{W}(\|p'_i - p_l\|_2; \sigma_s) + \varepsilon} f_i \quad (10)$$

where p_j denotes a neighboring point, $f'_i{}^{(s)}$ is the resampled feature, f_i is the original feature at p_i , σ_s is the Gaussian scale parameter for resampling, and ε is a small constant to avoid division by zero.

Notably, we deliberately omit the relative offset bias matrix in the resampling stage. In 2D image deformable convolutions, offset operations disrupt the regular grid topology, thus requiring explicit bias compensation to preserve

local geometric consistency [22, 41]. However, point clouds inherently lack a fixed grid structure. Rather than imposing biased terms, we allow the network to directly learn from the raw coordinate geometry, enabling more natural spatial deformation.

Gaussian-based Differentiable Reordering (GDR). Traditional sorting operations can explicitly reorder point indices but are inherently non-differentiable, blocking gradient flow and preventing end-to-end optimization of sequence sorting [9, 22]. To overcome this limitation, we reinterpret sorting as a continuous probabilistic mapping and design the Gaussian-based differentiable reordering mechanism according to Eq. (8), which maps discrete ranking relations into a continuous probabilistic space. Instead of assigning each token to a single discrete index, its sorting position is represented as a continuous Gaussian-weighted distribution over adjacent sequence locations, as illustrated in Fig. 2(e).

Specifically, we add the token offsets Δt to the base index vector $I \in \mathbb{R}^{N \times 1}$ (derived from the Hilbert curve) to obtain the shifted index vector s . We then compute the pairwise difference between s and the target index vector $J = [1, 2, \dots, N]$, forming a difference matrix $(s - J) \in \mathbb{R}^{N \times N}$. This matrix encodes the relative positional deviation between tokens, which is then used to perform Gaussian-weighted aggregation for differentiable reordering:

$$s_i = I_i + \Delta t_i, \quad (11)$$

$$f'_i{}^{(t)} = \sum_{j=1}^N \frac{\mathcal{W}(s_i - J_j; \sigma_t)}{\sum_{l=1}^N \mathcal{W}(s_i - J_l; \sigma_t) + \varepsilon} F'_i{}^{(s)} \quad (12)$$

where $f'_i{}^{(t)}$ denotes the reordered i -th token feature, $F'^{(s)}$ is the global resampled feature matrix obtained by stacking all local resampled features $\{f'_i{}^{(s)}\}_{i=1}^N$ from the GKR, and σ_t is the learnable Gaussian scale parameter controlling the smoothness of sorting.

During Gaussian-weighted aggregation, token features are softly distributed across neighboring sequence positions, forming a continuous and differentiable relaxation of discrete sorting. Importantly, GDR does not replace non-differentiable sorting but fully subsumes it within a continuous framework (See Appendix for detailed derivation.):

- When $\sigma_t \rightarrow +\infty$, GDR degenerates into global average pooling, with gradients vanishing as the derivative converges to zero everywhere.
- For any fixed $\sigma_t > 0$, the normalized Gaussian weights remain continuous and differentiable with respect to s_i , ensuring smooth gradient propagation and enabling end-to-end optimization.
- As $\sigma_t \rightarrow 0^+$, the mapping converges to deterministic sorting, where each position s_i inherits the feature of its nearest discrete index J_j , effectively snapping tokens to their closest sequence positions.

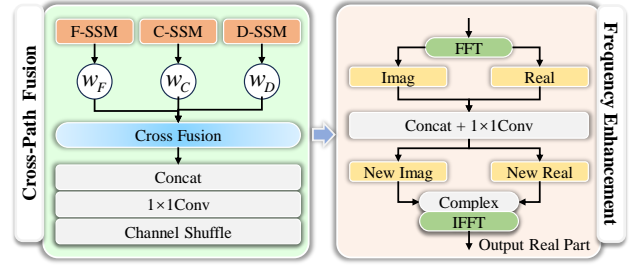


Figure 3. **Illustration of TPFF.** Cross-path fusion is performed first, followed by frequency enhancement.

Although token indices are not explicitly permuted, their features are nearly exchanged, achieving an effect equivalent to differentiable sorting. By controlling σ_t , GDR provides a smooth approximation to discrete ranking—smaller σ_t approximates standard sorting, while larger values approach global averaging—thus preserving the end-to-end learnability of token reordering.

In summary, deformable scanning enhances point cloud understanding by learning offsets that adaptively adjust point coordinates and scanning order across spatial and sequential domains. This design endows the model with strong geometric adaptability.

3.4. Tri-Path Frequency Fusion

In the DMB, the F-SSM, C-SSM, and D-SSM capture dynamic features along different pathways. Directly fusing these paths in the spatial domain may cause information redundancy, as signals of different paths overlap. To address this, we map the sequential features into the frequency domain, where cross-path information can be more effectively complemented (see Fig. 3).

The three pathway features, $F_F, F_C, F_D \in \mathbb{R}^{N \times D}$, are first adaptively modulated by the other two branches before cross-fusion:

$$w_i = \text{sigmoid}(F_i), \quad F'_i = F_i \odot \frac{1}{2}(w_j + w_k) \quad (13)$$

where (i, j, k) cyclically traverses $\{(F, C, D), (C, D, F), (D, F, C)\}$. This enables each pathway to perceive the activation strength of the others, allowing dynamic adjustment of their relative importance.

The modulated features are concatenated along the channel dimension (yielding $3D$ channels) and fused via a grouped convolution to reduce dimensionality back to D . To maintain inter-group communication, channel shuffle is applied after fusion:

$$F_{\text{shuffle}} = \text{shuffle}(\text{Conv}_{1 \times 1}([F'_F; F'_C; F'_D])) \quad (14)$$

We further perform adaptive enhancement in the frequency domain. Specifically, a Fast Fourier Transform

Table 1. **Classification on ModelNet40 and ScanObjectNN.** We report overall accuracy (%), number of parameters (#P), and FLOPs (#F). † denotes voting strategy.

Reference	Methods	ModelNet40 1k P	ScanObjectNN			#P(M)	#F(G)
			OBJ_BG	OBJ_ONLY	PB_T50_RS		
<i>Supervised Learning Only</i>							
CVPR 17	PointNet [3]	89.2	73.3	79.2	68.0	3.5	0.5
NeurIPS 17	PointNet++ [29]	90.7	82.3	84.3	77.9	1.5	1.7
TOG 19	DGCNN [36]	92.9	82.8	86.2	78.1	1.8	2.4
JAS 23	PointConT [23]	93.5	-	-	90.30	-	-
NeurIPS 24	PointMamba [17]	-	88.30	87.78	82.48	12.3	3.6
AAAI 25	PCM [49]	93.4	-	-	88.1	34.2	45.0
CVPR 25	SAST [1]	92.7	92.25	91.39	87.30	12.3	3.6
	DM3D	93.76	90.70	91.56	89.40	13.6	4.4
<i>With Self-supervised Pre-training</i>							
CVPR 22	Point-BERT† [45]	93.4	88.12	88.30	83.69	22.1	4.8
ECCV 22	Point-MAE† [28]	94.4	91.22	90.02	84.94	22.1	4.8
NeurIPS 23	PointGPT-S† [4]	94.0	91.6	90.0	86.9	29.2	5.7
CVPR 24	PointDif [52]	-	93.29	91.91	87.61	-	-
NeurIPS 24	PointMamba [17]	93.6	94.32	92.60	89.31	12.3	3.6
ACM MM 24	Mamba3D† [13]	95.1	95.18	92.60	93.34	16.9	3.9
NeuCom 25	E-Mamba [16]	94.7	94.32	92.94	91.98	13.78	7.49
ICCV 25	Point-PQAE [50]	94.0	95.0	93.6	89.6	22.1	-
CVPR 25	SAST [1]	93.4	94.32	91.91	89.10	12.3	3.6
	DM3D	94.53	94.32	93.72	93.09	13.6	4.4
	DM3D†	95.11	95.21	93.93	94.32	13.6	4.4

(FFT) is applied along the sequence dimension, followed by a 1×1 convolution on the real and imaginary components for frequency modulation, and finally, an inverse FFT (IFFT) reconstructs the spatial features. The overall process is formulated as:

$$F_{FFT} = \mathcal{F}(F_{shuffle}) = \Re(F_{FFT}) + i\Im(F_{FFT}) \quad (15)$$

$$[F_{FFT}^r; F_{FFT}^i] = Conv_{1 \times 1}([\Re(F_{FFT}); \Im(F_{FFT})]) \quad (16)$$

$$F_{out} = \Re(\mathcal{F}^{-1}(F_{FFT}^r + iF_{FFT}^i)) \quad (17)$$

where \mathcal{F} and \mathcal{F}^{-1} denote the FFT and IFFT, respectively. \Re and \Im represent the real and imaginary parts.

The TPFf projects spatial features from all SSM branches into a unified frequency domain to mitigate aliasing across overlapping receptive fields.

4. Experiments

4.1. Implementation Details

All experiments are conducted on a single NVIDIA TITAN RTX GPU. We set the total number of stages T to 6, the hidden dimension D to 384, the number of points N sampled by FPS to 128, and the number of neighbors K in KNN to 32. In the GKR, K_r is set to 3 and σ_s to 1, while in the GDR, σ_t is set to 0.2. The models are trained for 300

epochs using the AdamW optimizer with the cosine learning rate scheduler (CosLR), an initial learning rate of $5e-4$, weight decay of 0.05, warmup for 10 epochs, and batch size of 32. More parameter details are provided in the Appendix. The pre-training is conducted on ShapeNetCore [2], following prior protocols [13, 28, 42, 45]. Both classification and part segmentation adopt the cross-entropy loss.

4.2. Downstream Tasks

Classification. We adopt a three-layer MLP as the classification head and evaluate our method on ModelNet40 [40] and ScanObjectNN [31]. ModelNet40 uses 1024 input points with scale&translate augmentation, while ScanObjectNN uses 2048 points with rotation augmentation. As shown in Tab. 1, DM3D achieves highly competitive results. Without pre-training, it achieves 93.76% on ModelNet40 and 89.40% on PB_T50_RS, outperforming baselines such as PointMamba [17] and PCM [49], demonstrating strong robustness to perturbations. With pre-training, DM3D attains 93.09% overall accuracy (OA) on PB_T50_RS without voting, surpassing recent counterparts, including Point-PQAE [50] (89.6%) and SAST [1] (89.1%). Moreover, DM3D remains significantly more lightweight than PointGPT-S [4] and PCM [49], with only a minimal increase in computational cost.

Table 2. **Few-shot classification on ModelNet40 dataset.** A_{std} represents the average (A) and standard deviation (std) of OA.

Methods	5-Way		10-Way	
	10-Shot	20-Shot	10-Shot	20-Shot
<i>Supervised Learning Only</i>				
PointNet [3]	52.0 _{3.8}	57.8 _{4.9}	46.6 _{4.3}	35.2 _{4.8}
DGCNN [36]	31.6 _{2.8}	40.8 _{4.6}	19.9 _{2.1}	16.9 _{1.5}
OcCo [33]	90.6 _{2.8}	92.5 _{1.9}	82.9 _{1.3}	86.5 _{2.2}
DM3D	91.0 _{6.9}	94.8 _{3.6}	86.1 _{5.5}	91.75 _{3.2}
<i>With Self-supervised Pre-training</i>				
ACT [8]	96.8 _{2.3}	98.0 _{1.4}	93.3 _{4.0}	95.6 _{2.8}
Point-BERT [45]	94.6 _{3.1}	96.3 _{2.7}	91.0 _{5.4}	92.7 _{5.1}
Point-MAE [28]	96.3 _{2.5}	97.8 _{1.8}	92.6 _{4.1}	95.0 _{3.0}
PointGPT-S [4]	96.8 _{2.0}	98.6 _{1.1}	92.6 _{4.6}	95.2 _{3.4}
PointMamba [17]	95.0 _{2.3}	97.3 _{1.8}	91.4 _{4.4}	92.8 _{4.0}
DM3D	95.9 _{4.5}	97.5 _{3.2}	91.25 _{5.1}	95.7 _{3.0}

Table 3. **Part segmentation on the ShapeNetPart.** We reports class-level mIoU (Cls.mIoU) and instance-level mIoU (Ins.mIoU).

Method	Cls.mIoU(%)	Ins.mIoU(%)
<i>Supervised Learning Only</i>		
PointNet [3]	80.4	83.7
PointNet++ [29]	81.9	85.1
DGCNN [36]	82.3	85.2
DM3D	83.7	85.3
<i>With Self-supervised Pre-training</i>		
OcCo [33]	83.4	84.7
ACT [8]	84.7	86.2
MaskPoint [21]	84.6	86.0
Point-BERT [45]	84.1	85.6
Point-MAE [28]	84.2	86.1
PointMamba [17]	84.4	86.0
Mamba3D [13]	83.6	85.6
Point-PQAE [50]	84.6	86.1
DM3D	84.6	86.2

Few-shot Learning. We conduct few-shot classification experiments following prior work [13, 17, 20, 45] to further validate the few-shot learning capability of DM3D. As shown in Tab. 2, DM3D consistently outperforms other methods under the purely supervised setting, demonstrating strong feature learning capability. With pre-training, DM3D remains highly competitive, matching or surpassing Transformer-based methods, which highlights its robustness and generalization.

Part Segmentation. ShapeNetPart [2] contains 50 part categories across 16 object classes. We adopt 2048 input points without normals, and the segmentation head follows a PointNet++-like [29] design that extracts features from the 2nd, 4th, and 6th encoder layers. Tab. 3 shows that ShapeNetPart is extremely challenging, and even state-of-

Table 4. **Ablation on model architecture and components of deformable scanning.**

Method	OBJ_ONLY	PB_T50_RS	#P (M)	#F (G)
<i>(a) Ablation on model architecture</i>				
★ Full	91.56	89.40	13.6	4.4
w/o D-SSM	88.28	85.45	8.89	3.04
w/o TPF	90.74	88.52	13.39	4.38
<i>(b) Ablation on deformable scanning components</i>				
w/o LCFA	90.26	88.93	12.71	3.47
w/o OffsetNet	88.71	86.93	13.59	4.4
w/o GKR	89.12	86.08	13.6	4.4
w/o GDR	89.93	88.12	13.59	4.4

the-art methods only marginally improve compared to each other. With pre-training, DM3D achieves 84.6% Cls.mIoU and 86.2% Ins.mIoU. This surpasses the PointMamba baseline by 0.2% and matches or slightly outperforms recent methods such as Mamba3D [13] and Point-PQAE [50], validating that our deformable mechanism strengthens SSMs in capturing fine-grained geometric details. Visual results are provided in the Appendix.

4.3. Ablation Studies

To comprehensively evaluate the effectiveness of each component, we conduct ablation studies on the model architecture and its variants, with all trained from scratch.

Effect of Each Component. As shown in Tab. 4, the full model significantly outperforms all ablated variants on both tasks. Removing the deformable branch (w/o D-SSM) or the frequency fusion module (w/o TPF) leads to performance drops of 3.28%/3.95% and 0.82%/0.88%, respectively, confirming the effectiveness of the deformable mechanism and the importance of cross-path feature interaction.

We further ablate the components of deformable scanning. Removing LCFA causes performance drops of 1.3% and 0.47% on OBJ_ONLY and PB_T50_RS respectively, indicating that neighborhood aggregation provides richer contextual cues for offset prediction. Eliminating coordinate offsets causes a 2.85% drop, showing that spatial deformation enhances structural perception. Removing the GKR leads to 2.4% degradation, as the model loses the ability to capture new local structures. Similarly, removing the GDR yields a 1.4% performance loss, as it fails to prioritize scanning similar structures. These results demonstrate that our method improves performance in point cloud understanding, validating our design choices.

Effect of resampling neighborhood size K_r . K_r defines the resampling neighborhood after offset. Smaller values cause insufficient local aggregation, while larger ones introduce irrelevant points. As shown in Tab. 5(a), $K_r = 3$ offers the best trade-off. In contrast, K_q in LCFA only indirectly influences final performance, and the computational cost increases linearly with its value. Therefore, $K_q = 8$ is

Table 5. **Ablation on key parameters and fusion strategies.** We evaluate the effects of neighborhood size K_r in GKR, reordering methods and Gaussian scale σ_t in GDR, and path fusion strategies.

Variants	OBJ_ONLY	PB_T50_RS
<i>(a) Neighborhood size K_r in GKR.</i>		
$K_r = 2$	91.40	89.27
$K_r = 3$ (ours)	91.56	89.40
$K_r = 4$	91.35	89.21
$K_r = 5$	91.23	89.33
<i>(b) Reordering methods and Gaussian scale σ_t in GDR.</i>		
Fixed order (Hilbert)	89.93	88.12
Non-differentiable sorting	90.81	89.01
GDR ($\sigma_t=0.1$)	91.35	89.32
GDR ($\sigma_t=0.2$, ours)	91.56	89.40
GDR ($\sigma_t=0.4$)	91.23	89.29
GDR ($\sigma_t=0.6$)	91.12	89.04
<i>(c) Path fusion strategies.</i>		
Element-wise mean	90.74	88.52
Learned linear fusion	90.05	88.63
Convolutional fusion	89.86	87.42
TPFF (ours)	91.56	89.40

fixed for efficiency.

Effect of reordering methods and scale σ_t . Removing reordering or replacing GDR with a non-differentiable sorting operation causes 1.63%/1.28% and 0.75%/0.36% drops, respectively, confirming the necessity of dynamic sequence adjustment. While non-differentiable sorting introduces index reordering, its lack of gradient flow makes it inferior to GDR, which directly optimizes token shifts. Among GDR, the best result is achieved at $\sigma_t = 0.2$, where smaller values make the sorting overly strict and larger ones oversmooth discriminative features.

Effect of fusion schemes. We compare multiple path fusion strategies and observe that frequency fusion consistently surpasses spatial ones. Element-wise mean and linear fusions offer limited capacity for cross-path complementarity, while convolutional fusion insufficiently mitigates aliasing.

4.4. Visualization and Analysis

To better demonstrate the working effect of the deformable scan, we perform a visual analysis as shown in Fig. 4.

Analysis of Coordinate Offset. Larger offsets are observed near object boundaries, where richer geometric variations exist (see Fig. 4(a)). This indicates that the model learns to shift points toward—and focus resampling on—these semantically salient areas, thereby enhancing its sensitivity to fine structural details.

Analysis of Differentiable Reordering. The heatmap in Fig. 4(b) shows that each token is assigned a continuous

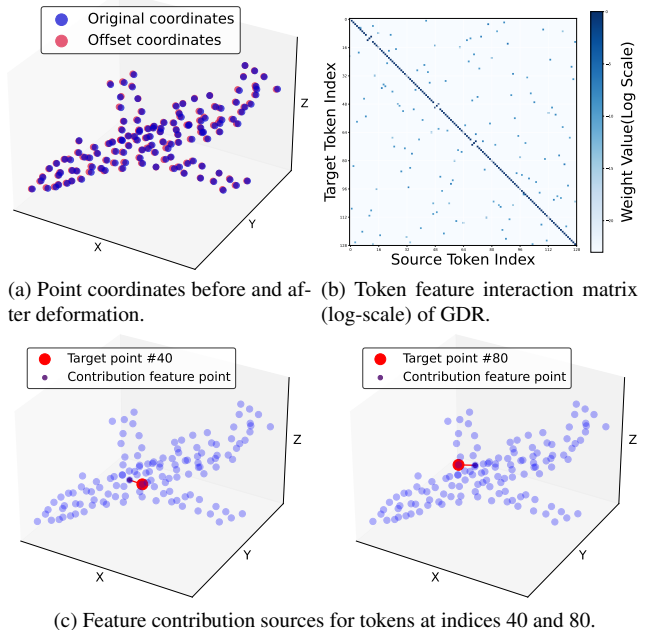


Figure 4. **Visualization of the deformable mechanism.** The token feature interaction matrix shows the feature weights from source tokens (x -axis) to target tokens (y -axis).

Gaussian-weighted distribution over target positions rather than a single discrete index, confirming that GDR performs probabilistic rather than deterministic reordering. Most weights concentrate along the main diagonal, indicating that GDR preserves global stability while allowing local flexibility; scattered off-diagonal activations indicate feature correlations between points. Target points receive contributions from neighboring points that share geometric or semantic similarities (see Fig. 4(c)). This encourages similar points to occupy adjacent sequence positions and prevents structural disruption caused by sorting, thereby maintaining local consistency.

5. Conclusion

In this paper, we propose DM3D, a deformable Mamba network for point cloud understanding. Unlike previous models that rely on fixed serialization, DM3D introduces an offset-guided deformable mechanism with Gaussian weighting, unifying local resampling and global reordering, and enabling end-to-end optimization of geometric structures and scanning paths. Extensive experiments on ModelNet40, ScanObjectNN, and ShapeNetPart demonstrate state-of-the-art performance, confirming that point cloud serialization should be learned and adapted as part of the model rather than treated as a static preprocessing step. While DM3D achieves compelling results, it introduces moderate efficiency overhead on extremely large-

scale point clouds owing to the deformable operations. Future work will explore more lightweight formulations to improve efficiency in large-scale scenarios.

References

- [1] Ali Bahri, Moslem Yazdanpanah, Mehrdad Noori, Sahar Dastani, Milad Cheraghalikhani, Gustavo Adolfo Vargas Hakim, David Osowiechi, Farzad Beizae, Ismail Ben Ayed, and Christian Desrosiers. Spectral informed mamba for robust point cloud processing. In *CVPR*, pages 11799–11809, 2025. 6
- [2] Angel Chang, Thomas Funkhouser, Leonidas Guibas, Pat Hanrahan, Qixing Huang, Zimo Li, Silvio Savarese, Manolis Savva, Shuran Song, Hao Su, Jianxiong Xiao, Li Yi, and Fisher Yu. Shapenet: An information-rich 3d model repository. *arXiv preprint arXiv:1512.03012*, 2015. 6, 7
- [3] R. Q. Charles, H. Su, M. Kaichun, and L. J. Guibas. Pointnet: Deep learning on point sets for 3d classification and segmentation. In *CVPR*, pages 77–85, 2017. 1, 6, 7
- [4] Guangyan Chen, Meiling Wang, Yi Yang, Kai Yu, Li Yuan, and Yufeng Yue. Pointgpt: Auto-regressively generative pre-training from point clouds. In *NeurIPS*, pages 29667–29679. Curran Associates, Inc., 2023. 6, 7
- [5] Yuwei Cheng, Jingran Su, Mengxin Jiang, and Yimin Liu. A novel radar point cloud generation method for robot environment perception. *IEEE Transactions on Robotics*, 38(6): 3754–3773, 2022. 1
- [6] Mingyue Cui, Junhua Long, Mingjian Feng, Boyang Li, and Huang Kai. Octformer: Efficient octree-based transformer for point cloud compression with local enhancement. In *AAAI*, pages 470–478, 2023. 1, 2
- [7] Jifeng Dai, Haozhi Qi, Yuwen Xiong, Yi Li, Guodong Zhang, Han Hu, and Yichen Wei. Deformable convolutional networks. In *ICCV*, pages 764–773, 2017. 2
- [8] Runpei Dong, Zekun Qi, Linfeng Zhang, Junbo Zhang, Jianjian Sun, Zheng Ge, Li Yi, and Kaisheng Ma. Autoencoders as cross-modal teachers: Can pretrained 2d image transformers help 3d representation learning? In *ICLR*, 2023. 7
- [9] Martin Engelberge, Louis Chevallier, Patrick Pérez, and Matthieu Cord. Sodeep: A sorting deep net to learn ranking loss surrogates. In *CVPR*, pages 10784–10793, 2019. 5
- [10] Albert Gu and Tri Dao. Mamba: Linear-time sequence modeling with selective state spaces. In *First Conference on Language Modeling*, 2024. 1, 2
- [11] Albert Gu, Isys Johnson, Karan Goel, Khaled Saab, Tri Dao, Atri Rudra, and Christopher Ré. Combining recurrent, convolutional, and continuous-time models with linear state space layers. In *NeurIPS*, pages 572–585. Curran Associates, Inc., 2021. 1
- [12] Albert Gu, Karan Goel, and Christopher Ré. Efficiently modeling long sequences with structured state spaces. In *ICLR*, 2022. 2
- [13] Xu Han, Yuan Tang, Zhaoxuan Wang, and Xianzhi Li. Mamba3d: Enhancing local features for 3d point cloud analysis via state space model. In *ACM MM*, pages 4995–5004. ACM, 2024. 1, 2, 3, 4, 6, 7
- [14] Tao Huang, Xiaohuan Pei, Shan You, Fei Wang, Chen Qian, and Chang Xu. Localmamba: Visual state space model with windowed selective scan. In *ECCV*, pages 12–22. Springer Nature Switzerland. 2
- [15] Alexander Kolesnikov, Alexey Dosovitskiy, Dirk Weissenborn, Georg Heigold, Jakob Uszkoreit, Lucas Beyer, Matthias Minderer, Mostafa Dehghani, Neil Houlsby, Sylvain Gelly, Thomas Unterthiner, and Xiaohua Zhai. An image is worth 16x16 words: Transformers for image recognition at scale. In *ICLR*, 2021. 3
- [16] Dengao Li, Zhichao Gao, Shufeng Hao, Ziyou Xun, Jiajian Song, Jie Cheng, and Jumin Zhao. E-mamba: An efficient mamba point cloud analysis method with enhanced feature representation. *Neurocomputing*, 639:130201, 2025. 2, 6
- [17] Dingkan Liang, Xin Zhou, Wei Xu, Xingkui Zhu, Zhikang Zou, Xiaoqing Ye, Xiao Tan, and Xiang Bai. Pointmamba: A simple state space model for point cloud analysis. In *NeurIPS*, pages 32653–32677. Curran Associates, Inc., 2024. 1, 2, 6, 7
- [18] Sohee Lim, Minwoo Shin, and Joonki Paik. Point cloud generation using deep adversarial local features for augmented and mixed reality contents. *IEEE Transactions on Consumer Electronics*, 68(1):69–76, 2022. 1
- [19] Zhi-Hao Lin, Sheng-Yu Huang, and Yu-Chiang Frank Wang. Convolution in the cloud: Learning deformable kernels in 3d graph convolution networks for point cloud analysis. In *CVPR*, pages 1797–1806, 2020. 2
- [20] Bin Liu, Chunyang Wang, Xuelian Liu, Bo Xiao, and Guan Xi. Hymamba: Mamba with hybrid geometry-feature coupling for efficient point cloud classification. *arXiv preprint arXiv:2505.11099*, 2025. 1, 3, 7
- [21] Haotian Liu, Mu Cai, and Yong Jae Lee. Masked discrimination for self-supervised learning on point clouds. In *ECCV*, pages 657–675, Cham, 2022. 7
- [22] Leiye Liu, Miao Zhang, Jihao Yin, Tingwei Liu, Wei Ji, Yongri Piao, and Huchuan Lu. Defmamba: Deformable visual state space model. In *CVPR*, pages 8838–8847, 2025. 2, 4, 5
- [23] Yahui Liu, Bin Tian, Yisheng Lv, Lingxi Li, and Fei-Yue Wang. Point cloud classification using content-based transformer via clustering in feature space. *IEEE/CAA Journal of Automatica Sinica*, 11(1):231, 2024. 6
- [24] Yue Liu, Yunjie Tian, Yuzhong Zhao, Hongtian Yu, Lingxi Xie, Yaowei Wang, Qixiang Ye, Jianbin Jiao, and Yunfan Liu. Vmamba: Visual state space model. In *NeurIPS*, pages 103031–103063. Curran Associates, Inc., 2024. 2
- [25] Zhijian Liu, Xinyu Yang, Haotian Tang, Shang Yang, and Song Han. Flatformer: Flattened window attention for efficient point cloud transformer. In *CVPR*, pages 1200–1211, 2023. 2
- [26] Dening Lu, Kyle Gao, Jonathan Li, Dedong Zhang, and Linlin Xu. Exploring token serialization for mamba-based lidar point cloud segmentation. *IEEE Transactions on Geoscience and Remote Sensing*, 63:1–14, 2025. 2
- [27] Dening Lu, Linlin Xu, Jun Zhou, Kyle Gao, Zheng Gong, and Dedong Zhang. 3d-umamba: 3d u-net with state space model for semantic segmentation of multi-source LiDAR

- point clouds. *International Journal of Applied Earth Observation and Geoinformation*, 136:104401, 2025. 2
- [28] Yatian Pang, Wenxiao Wang, Francis E. H. Tay, Wei Liu, Yonghong Tian, and Li Yuan. Masked autoencoders for point cloud self-supervised learning. In *ECCV*, pages 604–621, Cham, 2022. 6, 7
- [29] Charles Ruizhongtai Qi, Li Yi, Hao Su, and Leonidas J Guibas. Pointnet++: Deep hierarchical feature learning on point sets in a metric space. In *NeurIPS*. Curran Associates, Inc., 2017. 6, 7
- [30] Hugues Thomas, Charles R. Qi, Jean-Emmanuel Deschaud, Beatriz Marcotegui, François Goulette, and Leonidas Guibas. Kpconv: Flexible and deformable convolution for point clouds. In *ICCV*, pages 6410–6419, 2019. 2
- [31] Mikaela Angelina Uy, Quang-Hieu Pham, Binh-Son Hua, Thanh Nguyen, and Sai-Kit Yeung. Revisiting point cloud classification: A new benchmark dataset and classification model on real-world data. In *ICCV*, pages 1588–1597, 2019. 6
- [32] Ashish Vaswani, Noam Shazeer, Niki Parmar, Jakob Uszkoreit, Llion Jones, Aidan N. Gomez, Lukasz Kaiser, and Illia Polosukhin. Attention is all you need. In *NeurIPS*, page 6000–6010, Red Hook, NY, USA, 2017. Curran Associates Inc. 2
- [33] H. Wang, Q. Liu, X. Yue, J. Lasenby, and M. J. Kusner. Unsupervised point cloud pre-training via occlusion completion. In *ICCV*, pages 9762–9772, 2021. 7
- [34] Peng-Shuai Wang. Octformer: Octree-based transformers for 3d point clouds. *ACM Trans. Graph.*, 42(4), 2023. 1
- [35] Xinjie Wang, Yifan Zhang, Ting Liu, Xipu Liu, Ke Xu, Jianwei Wan, Yulan Guo, and Hanyun Wang. Topnet: Transformer-efficient occupancy prediction network for octree-structured point cloud geometry compression. In *CVPR*, pages 27305–27314, 2025. 1
- [36] Yue Wang, Yongbin Sun, Ziwei Liu, Sanjay E. Sarma, Michael M. Bronstein, and Justin M. Solomon. Dynamic graph cnn for learning on point clouds. *ACM Trans. Graph.*, 38(5), 2019. 1, 6, 7
- [37] Wenxuan Wu, Zhongang Qi, and Li Fuxin. Pointconv: Deep convolutional networks on 3d point clouds. In *CVPR*, pages 9613–9622, 2019. 2
- [38] Xiaoyang Wu, Yixing Lao, Li Jiang, Xihui Liu, and Hengshuang Zhao. Point transformer v2: Grouped vector attention and partition-based pooling. In *NeurIPS*, 2022. 2
- [39] Xiaoyang Wu, Li Jiang, Peng-Shuai Wang, Zhijian Liu, Xihui Liu, Yu Qiao, Wanli Ouyang, Tong He, and Hengshuang Zhao. Point transformer v3: Simpler, faster, stronger. In *CVPR*, pages 4840–4851, 2024. 2
- [40] Zhirong Wu, Shuran Song, Aditya Khosla, Fisher Yu, Linguang Zhang, Xiaoou Tang, and Jianxiong Xiao. 3d shapenets: A deep representation for volumetric shapes. In *CVPR*, pages 1912–1920, 2015. 6
- [41] Zhuofan Xia, Xuran Pan, Shiji Song, Li Erran Li, and Gao Huang. Vision transformer with deformable attention. In *CVPR*, pages 4784–4793, 2022. 2, 4, 5
- [42] Chenhongyi Yang, Zehui Chen, Miguel Espinosa, Linus Ericsson, Zhenyu Wang, Jiaming Liu, and Elliot J. Crowley. Plainmamba: Improving non-hierarchical mamba in visual recognition. In *35th British Machine Vision Conference (BMVC)*, 2024. 2, 3, 4, 6
- [43] Yulong Yang, Tianzhou Xun, Kuangrong Hao, Bing Wei, and Xue-song Tang. Grid mamba: grid state space model for large-scale point cloud analysis. *Neurocomputing*, 636: 129985. 1, 2, 4
- [44] Weihao Yu and Xinchao Wang. Mambaout: Do we really need mamba for vision? In *CVPR*, pages 4484–4496, 2025. 2, 4
- [45] Xumin Yu, Lulu Tang, Yongming Rao, Tiejun Huang, Jie Zhou, and Jiwen Lu. Point-bert: Pre-training 3d point cloud transformers with masked point modeling. In *CVPR*, pages 19291–19300, 2022. 3, 6, 7
- [46] Kang Zeng, Hao Shi, Jiacheng Lin, Siyu Li, Juntao Cheng, Kaiwei Wang, Zhiyong Li, and Kailun Yang. Mambamos: Lidar-based 3d moving object segmentation with motion-aware state space model. *arXiv preprint arXiv:2404.12794*, 2024. 1
- [47] Guowen Zhang, Lue Fan, Chenhang He, Zhen Lei, Zhaoxiang Zhang, and Lei Zhang. Voxel mamba: group-free state space models for point cloud based 3d object detection. In *NeurIPS*, Red Hook, NY, USA, 2024. Curran Associates Inc. 2
- [48] Lunjun Zhang, Anqi Joyce Yang, Yuwen Xiong, Sergio Casas, Bin Yang, Mengye Ren, and Raquel Urtasun. Towards unsupervised object detection from lidar point clouds. In *CVPR*, pages 9317–9328, 2023. 1
- [49] Tao Zhang, Haobo Yuan, Lu Qi, Jiangning Zhang, Qianyu Zhou, Shunping Ji, Shuicheng Yan, and Xiangtai Li. Point cloud mamba: Point cloud learning via state space model. In *AAAI*, pages 10121–10130, 2025. 1, 2, 6
- [50] Xiangdong Zhang, Shaofeng Zhang, and Junchi Yan. Towards more diverse and challenging pre-training for point cloud learning: Self-supervised cross reconstruction with decoupled views. In *ICCV*, 2025. 6, 7
- [51] Hengshuang Zhao, Li Jiang, Jiaya Jia, Philip Torr, and Vladlen Koltun. Point transformer. In *ICCV*, pages 16239–16248, 2021. 1
- [52] Xiao Zheng, Xiaoshui Huang, Guofeng Mei, Yuenan Hou, Zhaoyang Lyu, Bo Dai, Wanli Ouyang, and Yongshun Gong. Point cloud pre-training with diffusion models. In *CVPR*, pages 22935–22945, 2024. 6
- [53] Zixiang Zhou, Xiangchen Zhao, Yu Wang, Panqu Wang, and Hassan Foroosh. Centerformer: Center-based transformer for 3d object detection. In *ECCV*, 2022. 2
- [54] Lianghui Zhu, Bencheng Liao, Qian Zhang, Xinlong Wang, Wenyu Liu, and Xinggang Wang. Vision mamba: Efficient visual representation learning with bidirectional state space model. In *ICML*, pages 62429–62442, 2024. 2